Wind turbine noise propagation in flat terrain for wind farm layout optimization frameworks

Sessarego, Matias; Shen, Wen Zhong; Barlas, Emre

Published in:
Proceedings of the 8th International Conference on Wind Turbine Noise

Publication date:
2019

INCEEUROPE

8th International Conference
on
Wind Turbine Noise
Lisbon – 12th to 14th June 2019

Wind turbine noise propagation in flat terrain for wind farm layout optimization frameworks

Matias Sessarego
Department of Wind Energy, Technical University of Denmark, Nils Koppels Allé, 2800 Kongens Lyngby, Denmark

Wen Zhong Shen
Department of Wind Energy, Technical University of Denmark, Nils Koppels Allé, 2800 Kongens Lyngby, Denmark

Emre Barlas
Goldwind Denmark, Delta 4, 8382 Hinnerup, Denmark

Summary

This paper describes the wind turbine noise propagation in flat terrain for use in wind farm layout optimization frameworks. Large-eddy simulations of a single wind turbine in flat terrain at varying wind speeds, shear and turbulence levels are performed. The wind turbine is modeled using an actuator line approach, while the wind turbine noise propagation is computed using the Technical University of Denmark's WindSTAR-Pro (Wind turbine Simulation Tool for AeRodynamic noise Propagation). The wind turbine noise propagation is computed in a quasi-three-dimensional manner by using a two-dimensional (2D) parabolic equation (PE) model at numerous 2D-planes around the wind turbine. In this study, the 2D, wide-angle, Crank-Nicholson PE model is used. The relative sound pressure level obtained from WindSTAR-Pro around the wind turbine is computed for varying wind speeds, shear and turbulence levels. Wind flow velocity and relative sound pressure levels for selected wind conditions are shown. The end goal is to create a noise propagation database that can be used as a lookup table in wind farm layout optimization frameworks to mitigate the noise impact in the development of new wind farms.

1. Introduction

According to the Nordic Energy Technology Perspectives 2016 [1], a five-fold increase of wind energy generation is proposed in the Nordic countries by 2050 and two-thirds, i.e., 2/3, of Nordic wind energy generation will be placed onshore. For the people who may be affected, such as farmers and people living nearby wind turbines, the large amount of onshore wind penetration emphasizes the importance of public acceptance. One of the main obstacles in the public acceptance of wind energy is wind turbine noise [2]. Many studies have been carried out on the topic, e.g. the human response to wind turbine noise as well as the reasons for the higher annoyance of wind turbine noise compared to other noise sources [3, 4]. Consequently, regulations have been put forth, such as the Danish wind turbine noise regulation [5] that limits the noise impact from wind turbines. Such regulations, however, may have an adverse effect on the energy yield of wind farms and limit the number of new wind farms being developed on land. Therefore, there is a need to develop wind farm design tools that include the noise emission to mitigate wind farm noise without compromising on energy yield and onshore wind farm development.

The following sections describe a wind turbine flow solver coupled to a noise propagation tool, which is then used for modeling wind turbine noise propagation in flat terrain for use in wind farm layout optimization frameworks. The relative sound pressure level (SPL) is computed for different inflow cases, i.e., varying wind speeds, shear and turbulence levels. The entire process of simulating the flow and noise is automated in a way that it becomes easy to generate a large number of relative SPL results for the different inflow cases. The end goal is to create a noise propagation database that can be used as a lookup table in wind farm layout optimization frameworks, e.g. [6], to mitigate the noise impact in the development of new wind farms. Instead of the table-lookup, a surrogate model could be constructed based on the set of simulated inflow cases and incorporated in the framework as well. Such an approach was used for quick assessment of site-specific lifetime fatigue loads of wind turbines [7, 8]. Nevertheless, the focus of the current article is in the simulation of the individual inflow cases rather than the structure of the database and its implementation in the framework.

In the current article, the noise propagation database within a wind farm layout optimization context is kept as general as possible, thus noise generation is not considered. For the moment, the idea is to have the noise generation calculations performed at each iteration in the wind farm layout optimization framework instead, since noise generation calculations can be calculated relatively quickly using engineering models such as classic BPM [9] or Amiet's model [10]. In the near future, noise generation may be incorporated into the database. The primary purpose of the noise propagation database is to include higher-order propagation effects to the noise emission in an efficient manner. The integration of the noise generation and propagation tools in a wind plant layout optimization framework is currently under development.

Last, noise is generally an onshore problem, which is commonly over non-flat or complex terrain. Since the noise database is based on flat terrain, there is an inconsistency if the database is used for wind turbine layout optimization on complex terrain. In this scenario, the database should be treated as an approximation. Still, a database approach strictly for complex terrain may not be possible because of the infinite amount of different terrain topographies which must be considered. It is assumed that the user of the wind turbine layout optimization framework is aware of the inconsistency when analyzing the final results for complex terrain scenarios.

The article is structured into five sections. Section 2 describes the wind turbine flow solver that provides the necessary flow input for the noise propagation model described in Section 3. Wind

turbine noise propagation modeling under different inflow scenarios is described in Section 4. Finally, conclusions are provided in Section 5.

2. Wind turbine flow solver

Before the noise propagation computations are carried out, flow simulations are performed to provide the flow input to the noise propagation model. This section describes the simulation tool and models used to generate the flow inputs in two subsections. Subsection 2.1 describes the general purpose flow solver and subsection 2.2 describes the actuator line model used to represent the wind turbine within the flow domain. Subsection 2.3 describes the computational setup to execute the flow solver to obtain the flow fields.

2.1. Flow field

The flow is governed by the Navier-Stokes equations and simulations are performed using a computational fluid dynamics (CFD) solver typically based on either the Reynolds-Averaged Navier-Stokes (RANS) or Large-Eddy Simulation (LES). LES solvers are approximately three orders more computationally expensive than RANS solvers [11], since the large scale turbulence is resolved on a grid and only the smaller scale turbulence is modeled, e.g. using an eddy viscosity based sub-grid scale (SGS) model. RANS solvers are generally performed in a steady-state manner where all scales of turbulence are modeled [12]. The different turbulence scales in the flow are relevant because they are responsible for the noise generation in turbulent flow induced noise and have an impact on noise propagation. Flow fields from LES computations allows the noise propagation model to capture the effects of noise from some of the different turbulent scales.

The in-house EllipSys3D [13, 14] code developed at the Technical University of Denmark (DTU) is employed in the current work for generating the flow fields. EllipSys3D is a general purpose flow solver based on a structured grid topology, with a multi-block and cell-centered finite volume discretization. The Navier-Stokes equations are solved either steady or unsteady using the pressure-velocity coupling technique where the predictor-corrector method is used. In the predictor step, a second-order backward differentiation scheme is used as time discretization and a second-order central difference scheme is used as spatial discretization. The convective terms are discretized by the QUICK upwind scheme. Improved Rhie-Chow interpolation [15] is used in the corrector step to avoid numerical oscillations from the velocity-pressure decoupling. Besides the SIMPLE algorithm, the improved SIMPLEC scheme for collocated grids [16] is also implemented with the advantage that the solution is independent of the relaxation value. The EllipSys3D code is programmed with a multi-block topology and is parallelized using Message Passage Interface (MPI). Both the RANS and LES techniques are implemented in EllipSys3D, however only the filtered Navier-Stokes LES equations are being solved numerically in the current study. Last, only neutral atmospheric stability conditions are considered in the flow simulations.

2.2. Actuator line model

To include the effects of the wind turbine wake and unsteady moving sources on noise propagation, a wind turbine rotor model is required in the wind turbine flow solver. The actuator line (AL) technique as described in [17] is employed in the current work, where the wind turbine rotor blades are represented by rotating lines. By using the AL technique within EllipSys3D, complex flow

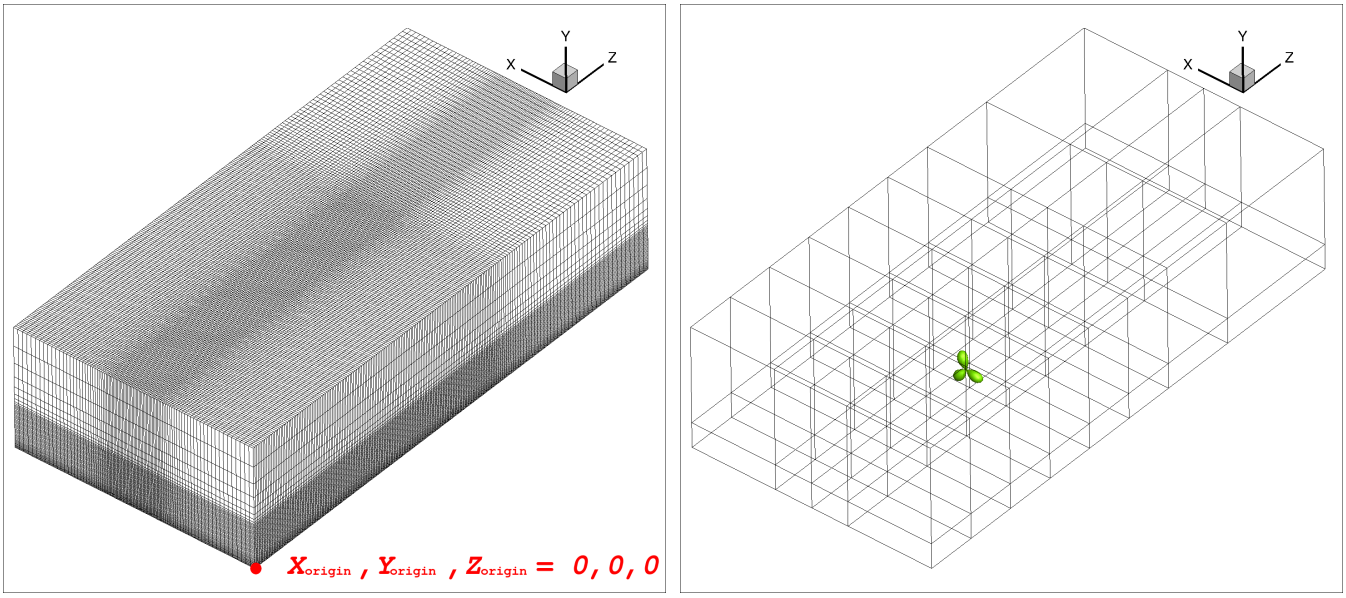

(a) **(b)**

Fig. 1 (a) Computational grid and (b) block structure used in the AL-LES computations. The three green spheroids in (b) represents the location of the actuator lines in the domain.

conditions on the wind turbine can be modeled, such as turbulent inflow, wind shear and yaw, etc. To compute the flow field over the wind turbine blades, a volume body force is added to the momentum equation. The body force is computed iteratively with the blade element approach with tabulated airfoil lift and drag data, e.g. lift (C_L) and drag (C_D) coefficients. The AL approach is coupled with the in-house developed aero-elastic code FLEX5 [18, 19]. The coupling with FLEX5 allows the addition of the wind turbine pitch and rotor RPM controllers as well as the flexibility of the turbine components, e.g. blades, tower, shaft, etc., within the simulation. However, for the purpose of this study, wind turbine control and flexibility are disabled. The focus is primarily on the noise propagation effects from different inflow conditions. The NREL 5 MW wind turbine [20] with a rotor diameter of 126 m and a hub height of 90 m is employed as the test turbine in the current study.

2.3. Flow solver setup

Figure 1 depicts the (a) computational grid and (b) block structure used in the flow-solver computations. In the flow solver setup, the mesh is a rectangular box with dimensions: width $\times$ height $\times$ length = $X_{\text{length}} \times Y_{\text{length}} \times Z_{\text{length}}$ = 1000 m $\times$ 500 m $\times$ 2000 m. The wind turbine rotor center is placed at X_{rotor} = 500 m, $Y_{\text{rotor}} = Y_H$ = 90 m, and Z_{rotor} = 800 m, where the origin of the mesh, X_{origin} = 0 m, Y_{origin} = 0 m, and Z_{origin} = 0 m, is defined in the bottom corner of the rectangular box as shown in Figure 1(a). The three green spheroids in Figure 1(b) represents the location of the rotor, or actuator lines, in the domain.

The mesh is comprised of 4 (horizontal) $\times$ 2 (vertical) $\times$ 8 (longitudinal) = 64 blocks with each block having 48^3 grid cells. The dimensions of all the 64 blocks are shown as black lines in Figure 1(b). Given an amount of computational resources to work with, since the amount of computational resources is limited, the computational mesh is designed such that there are more grid points upstream and downstream of the rotor location. Therefore, the sizes of the blocks are smaller in

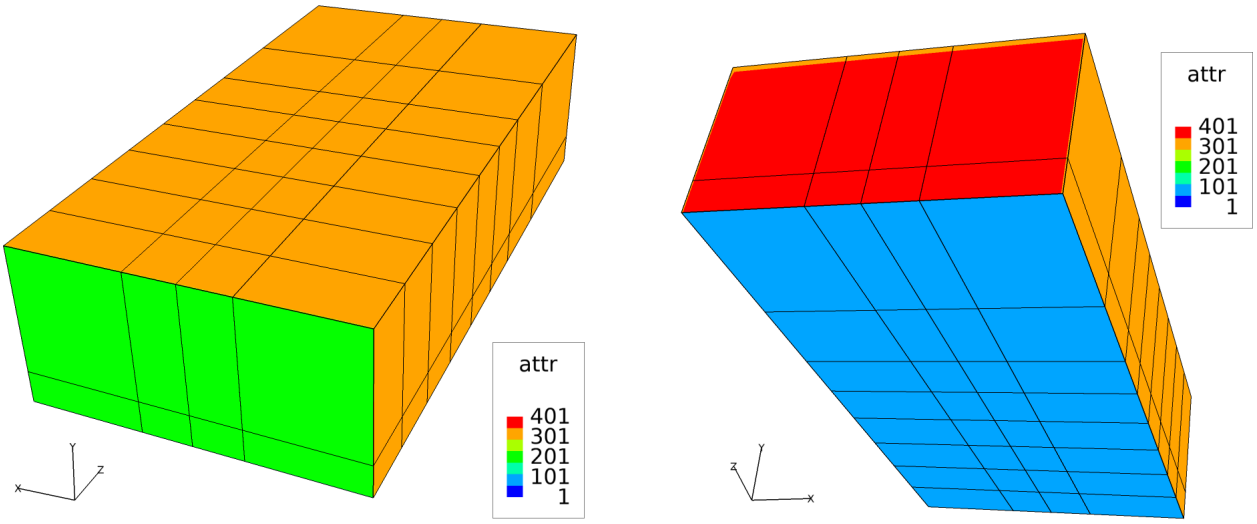

(a) (b)

Fig. 2 Two views of the boundary conditions applied on the mesh from the (a) front-top and (b) rear-bottom. No-slip, inlet, far-field, and outlet boundary conditions or attributes (attr) are color-coded as 101 (blue), 201 (green), 301 (orange), and 401 (red), respectively.

these regions as a means to increase the grid density. Upstream and downstream of the rotor, the velocity gradients will be the greatest and therefore the mesh should be refined accordingly. Further away from the rotor and towards the boundary of the mesh, a coarser grid is used to minimize the computational cost. There are approximately 50 (vertical) $\times$ 42 (horizontal) grid cells on the rotor swept area, which is similar to the number of grid cells used in Refs [18, 21]. The minimum/maximum grid cell lengths in the X, Y, and Z directions in the mesh are approximately 3.0 m/9.3 m, 1.4 m/40.0 m, and 4.2 m/11.4 m, respectively.

Figure 2 depicts two views of the boundary conditions applied on the mesh from the (a) front-top and (b) rear-bottom. No-slip, inlet, far-field, and outlet boundary conditions or attributes (attr) are color-coded as 101 (blue), 201 (green), 301 (orange), and 401 (red), respectively. The velocities for the inflow and far-field boundary conditions are prescribed. The fluid velocity for the no-slip boundary condition is zero.

Synthetic inflow turbulence is simulated by prescribing a plane, 1000 m (horizontal) $\times$ 500 m (vertical) in size, where the bottom-right corner of the plane lies at the origin of the mesh, i.e., $X_{\text{origin}} = 0$, $Y_{\text{origin}} = 0$, and $Z_{\text{origin}} = 0$. In other words, synthetic inflow turbulence is prescribed on the entire front-side of the mesh where the inlet boundary condition is also prescribed, see 201-green in Figure 2(a). Turbulence boxes are generated as a pre-processing step using the Mann model [22, 23] and slices from the box are gradually fed into the plane during the simulation. To capture the effect of each slice from the turbulence box in the AL-LES simulation, the resolution of the turbulence box should be slightly coarser than or equal to the resolution of the computational grid. A coarse resolution of approximately 8 meters/point (horizontal) $\times$ 8 meters/point (vertical) $\times$ 4.9 meters/point (longitudinal) was selected for the turbulence box. Due to the coarseness of the turbulence box, smaller turbulence scales that one could get from a finer turbulence box will not contribute to the flow solution. A finer turbulence box resolution will be used in the near

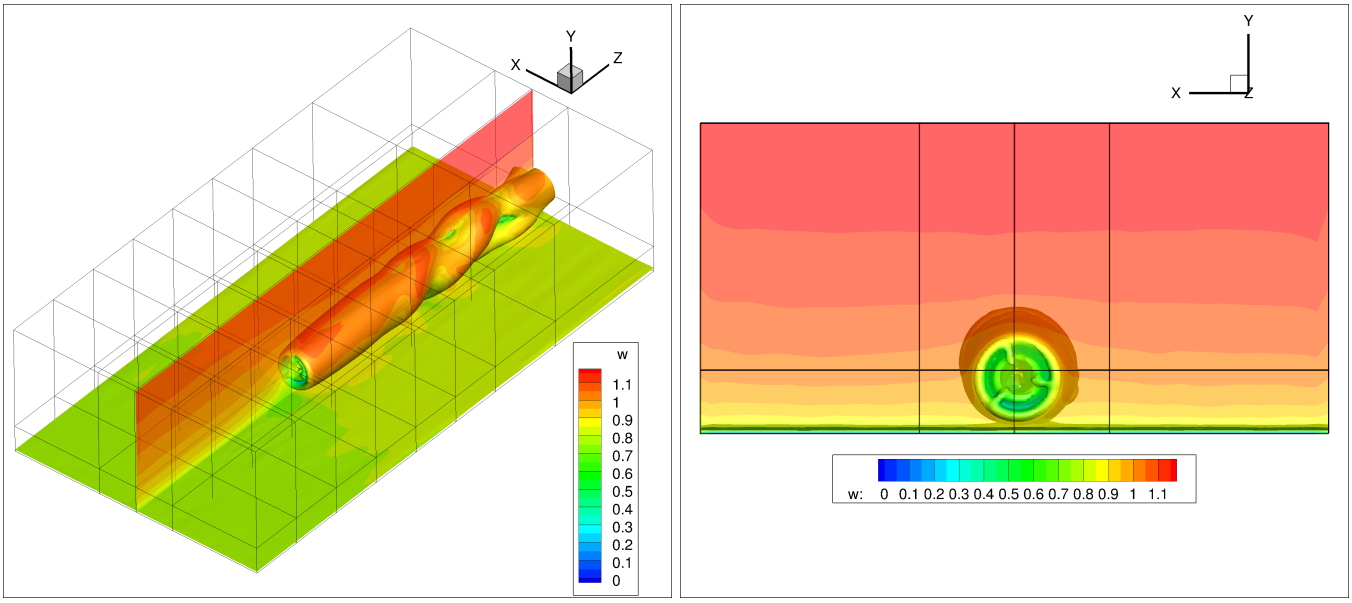

(a) **(b)**

Fig. 3 Two views of the iso-surface of vorticity from the actuator line large-eddy simulation in (a) three-dimensions and (b) from the front. Two-dimensional slices with normalized streamwise velocity, w, also shown.

future.

To simulate the wind shear, a prescribed wind profile power law is imposed everywhere in the domain at the first time-step in the AL-LES. Various shear exponents (ν) are used as defined by the parameter input range for the database. Using the coordinate system shown in Figures 1 to 2, the wind profile power law [24] is defined by Equation (1):

$$U(Y) = U_H \left(\frac{Y}{Y_H} \right)^{\nu} \tag{1}$$

where $U(Y)$ is the wind speed at height Y, U_H is the wind speed at hub height Y_H, and ν is a parameter giving the amount of shear.

Each AL-LES computation is performed using four nodes where each node contains twenty 2.8 GHz processors on a Linux cluster. The total number of processors is then 80, i.e., 4 nodes $\times$ 20 processors/node = 80 processors. However, for code execution efficiency, only 4 $\times$ 16 = 64 processors out of the 80 processors are used and each of the 64 processors is allocated one block out of the 64 blocks. The simulated real time for each simulation is 800 seconds including initial transients and requires approximately 19-24 hours for completion. Figure 3 depicts the result from an AL-LES computation in two views (a) and (b). In Figure 3, the iso-surface of vorticity in (a) three-dimensions and (b) from the front are shown. Two-dimensional slices with normalized streamwise velocity, w, are included in the figure as well. Figure 4 depicts the same as Figure 3 but for a simulation with an increased turbulence intensity. The iso-surface of vorticity in Figure 4 is adjusted to show the effect of the Mann turbulence box more clearly.

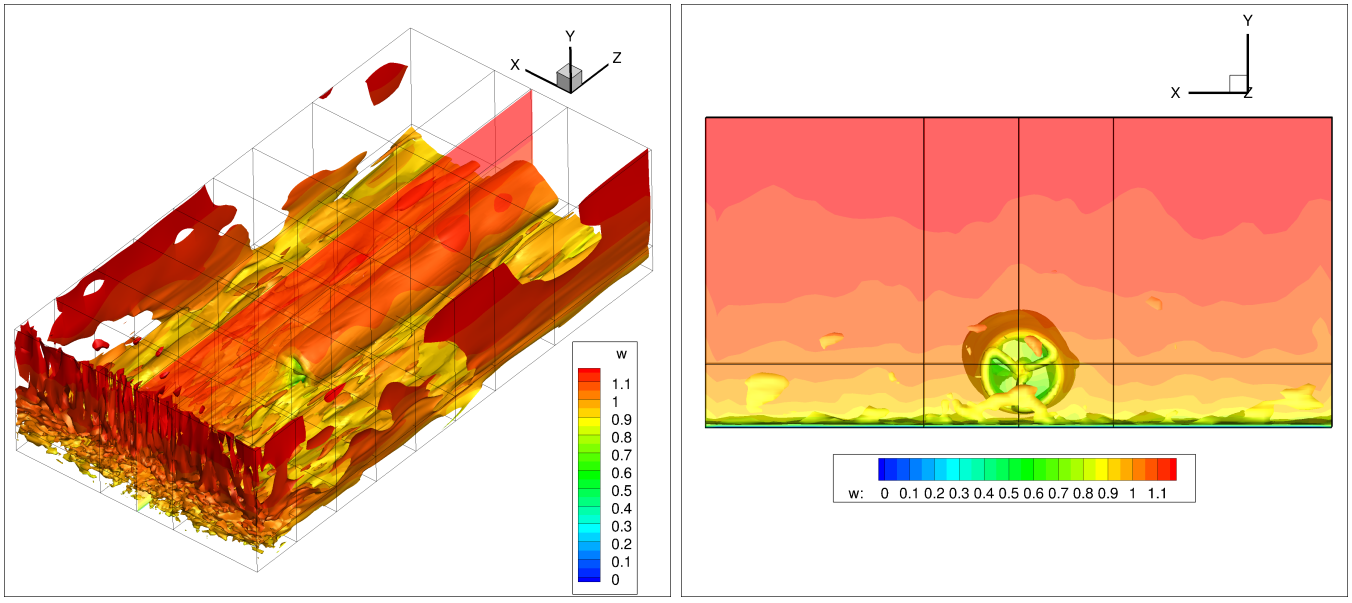

(a) **(b)**

Fig. 4 Two views of the iso-surface of vorticity from the actuator line large-eddy simulation with increased turbulence intensity in (a) three-dimensions and (b) from the front. Two-dimensional slices with normalized streamwise velocity, w, also shown.

3. Noise propagation solver

This section describes the noise propagation solver, WindSTAR-Pro [25, 26], in subsection 3.1 as well as the computational setup in subsection 3.2.

3.1. Noise propagation model

Predictions of wind turbine noise propagation can be made with various analytical and numerical modeling techniques, see [27] for a review. For example, there is a variety of ray tracing formulations available, which are analytical approaches based on geometrical acoustic theory. Due to the assumptions in geometrical acoustics, ray-tracing methods may not be the best method for low frequency noise propagation and generally cannot handle more complex atmospheric phenomena such as turbulence scattering, wind shear and diffraction effects. When considering more complicated terrain topography and/or atmospheric conditions, numerical approaches based on parabolic equations (PEs) are more suitable to the problem.

A two-dimensional (2D) PE model is employed in the current work as a compromise between simulation accuracy and computational cost. The PE method is a solution to the acoustic wave equation with approximations of harmonic wave propagations with a finite angle and a preferred direction of propagation. In this study, the 2D, wide-angle, Crank-Nicholson PE is used with the starter function and implementation details given in [28]. In this method the moving atmosphere is replaced by a hypothetical motionless medium with an effective speed of sound, $c_{eff} = c + v_x$, where v_x is the wind velocity component along the direction between source and receiver [29]. The wind velocity components are obtained from the flow solver described in Section 2. The solution of each PE simulation yields a steady solution at each frequency. Since a time dependent solution is desired in the present work, multiple PE simulations are performed successively to capture the relative sound pressure level as a function of time.

The PE model has limitations, but only some of them will be described here. First, the wide-angle implementation of the parabolic wave equation is only valid within ±35 degrees in the paraxial direction [25]. This limitation can be an issue for elevated sources like a wind turbine if the area of interest is close to both the ground and wind turbine. Second, the PE model is a one-way propagation method, which means that backscattering is neglected and results under multiple scattering are not reliable, e.g. a source between two noise barriers. Usually this is not the case for wind turbines though. Last, the 2D approach is another limitation. An axisymmetric approximation is employed here to reduce a 3D problem into 2D, which neglects azimuthal variations.

The PE model has been studied extensively by Barlas et al. [30–32] for single wind turbine noise propagation on flat terrain using a variety of inputs and simulation scenarios. In these studies, the effects of wind shear, different turbulence intensity levels and source modeling approaches are investigated. At DTU, the PE model is incorporated into a general purpose noise propagation tool called WindSTAR-Pro (Wind turbine Simulation Tool for AeRodynamic noise Propagation) [26].

3.2. Noise propagation setup

The PE model is coupled with a time varying sound source model. With this approach the flow solution and the location of the blades (or sources) at fifty time steps (or every 16 seconds of real-time) are extracted from the wind turbine flow solver. Preferably, the flow solution and blade locations should be extracted more frequently, e.g. every 0.2 seconds. However, such a small time step would generate a large amount of data and be more difficult to process. For the purpose of this study, a large time step is used which can be changed later on.

The flow field is extracted from the flow solution such as the ones shown in Section 2. Figure 5 depicts the extraction procedure for the streamwise wind velocity from the wind turbine flow solver for input to the noise propagation model. There are 801 slices from the domain normal to the streamwise direction that are extracted, but only twenty slices are shown in the figure for visibility. Since there are only 8 blocks $\times$ 48 cells/block = 384 cells in the streamwise direction, 801 slices might be about two times more than what is necessary and hence should be changed in the near future. The coordinate system shown in Figure 5 is different from Figures 1 to 4 because the EllipSys3D coordinate system labels during the extraction are modified to comply with the propagation model input coordinate system.

The sound emission from each wind turbine blade can be approximated by a lumped point source on the outer part of each blade, but not at the tip, e.g. at 80% of the blade span. This approximation is based on the source location studies in [2], which states that the sound is produced in the outer part of the blades. Therefore, the source locations are calculated based on 80% of the span of each actuator line. Figure 6 depicts the source locations shown on top of the streamwise wind velocity at time = 800 seconds in two views: (a) side view and (b) front view. The sources in Figure 6(a) are tilted because the NREL 5MW wind turbine has a shaft tilt of 5° [20].

Then, the relative sound pressure level is computed in a quasi-three-dimensional (quasi-3D) manner by performing 2D-PE simulations at numerous 2D planes within the domain and around the wind turbine. For the Crank-Nicholson PE calculations, the spatial resolution for both horizontal and vertical directions on the 2D-plane is set to one-eighth of the wavelength, i.e., $\delta x = \delta y = \lambda/8$, where λ is the wavelength of the solving frequency. Only flat terrain is considered and the ground impedance was defined using the theoretical and four-parameter model of Attenborough [33]. An

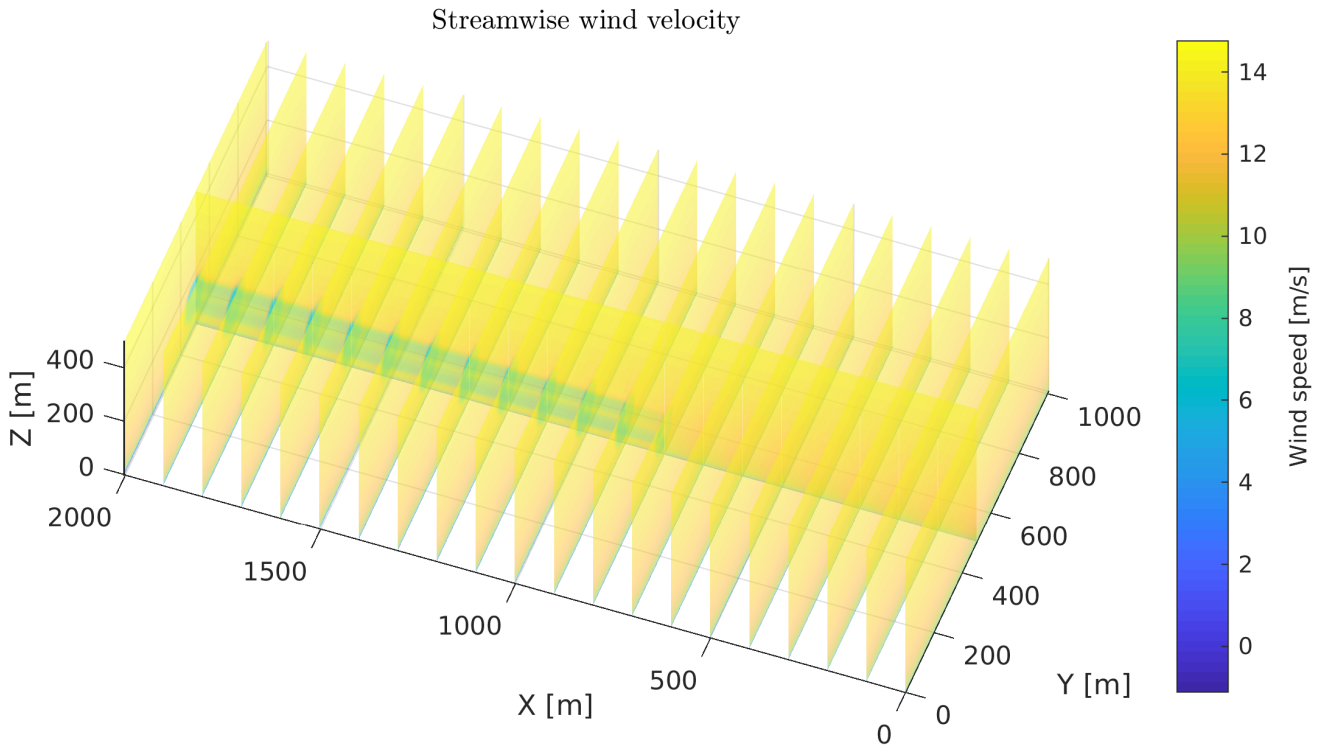

Fig. 5 Streamwise wind velocity extraction from flow solver for input to the noise propagation model. There are 801 slices from the domain that are extracted, but only twenty slices are shown for visibility. The coordinate system is modified for compatibility with the propagation model.

effective flow resistivity value of 200 kPa s/m^2 representative of grassland was chosen, which is the case where onshore wind turbines are commonly situated.

All simulations are carried out for 1/3 octave band center frequencies, f_i, from 50 Hz to 800 Hz. Frequencies higher than 800 Hz are assumed to have a negligible contribution to the overall SPL due to atmospheric absorption. Nevertheless, parameter settings can be easily changed and the simulations can be rerun if needed. The sound pressure level, L_p, is defined by Equation (2):

$$L_p(f_i) = L_W(f_i) - 10\log_{10} 4\pi r^2 - \alpha r + \Delta L \tag{2}$$

where L_W is the sound power level, α is the atmospheric absorption coefficient, r is the radial distance from the source, and ΔL is the relative sound pressure level. In the current study, only ΔL is considered in the analyses and the noise database. In other words, the sound power level, atmospheric absorption, and geometrical attenuation terms in Equation (2) are neglected. As mentioned in Section 1, noise generation or noise source, i.e., L_W, as well as the remaining terms in Equation (2) may be incorporated into the database in the near future. For now, only the relative sound pressure level in each band are summed logarithmically to obtain the overall relative sound pressure level, ΔL_{sum}, as defined in Equation (3):

$$\Delta L_{\text{sum}} = 10\log_{10}\left(\sum_{i=1}^{N} 10^{\Delta L/10}\right) \tag{3}$$

where N is the number of frequencies used.

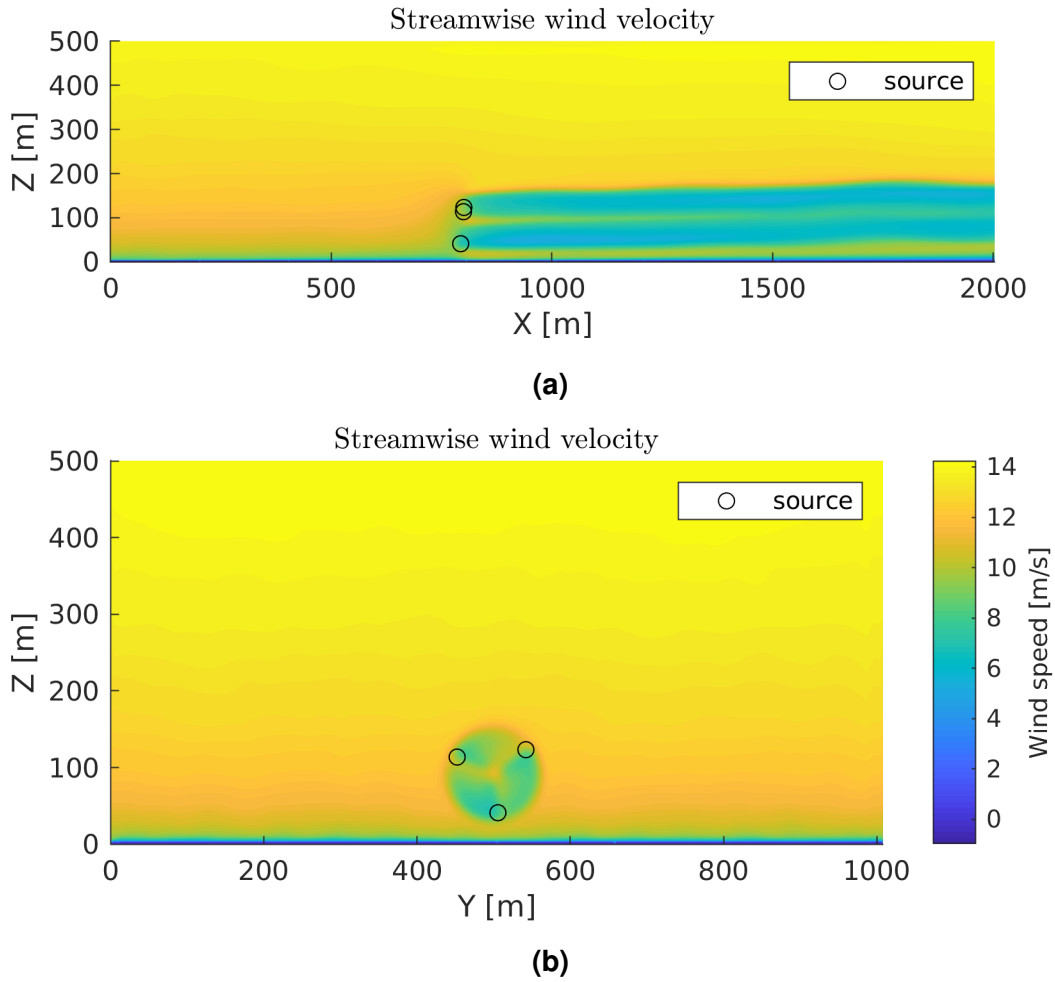

Fig. 6 Source locations shown on top of the streamwise wind velocity in two views: (a) side view and (b) front view.

4. Wind turbine noise propagation modeling

This section shows the computational results from the wind turbine noise propagation modeling based on the flow solution shown in Section 2. An excerpt from the noise propagation database is also shown in this section. Figure 7 depicts the two-dimensional planes from three sources (or three blades) to a receiver at X, Y, Z = (1950 m, 500 m, 2 m) with the (a) interpolated streamwise wind velocity flow field used in the PE model and (b) overall relative sound pressure levels computed from the PE model.

Figure 8 depicts the mean overall relative sound pressure levels, i.e. mean ΔL_{sum}, for the time period 640-800 seconds shown (a) on top of the receiver locations at 2 m height and (b) as a contour plot. The 640-800 second time period is a conservative choice to ensure that the wakes considered in the analyses have reached the end of the domain in the streamwise direction and is fully developed. Figure 9 depicts the wake at time = 80 seconds, which does not reach the end of the domain and is not fully developed like in Figure 6(a). There are a total of 1082 receiver locations that are used to construct a contour of rel. SPL for a given wind inflow condition. In the near future, the number of receiver locations might be halved since the contours are generally symmetric above and below the Y = 500 m axis in Figure 8(b).

As mentioned in Section 3.1, the PE model is only valid within ±35 degrees from the source in

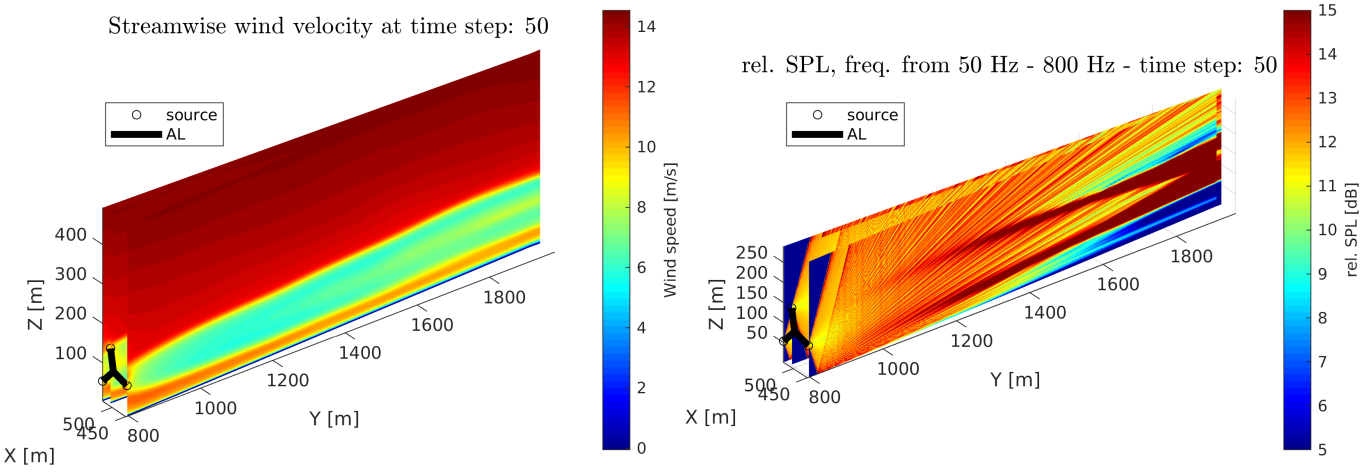

(a) (b)

Fig. 7 Two-dimensional planes from three sources (or three blades) to a receiver at X, Y, Z = (1950 m, 500 m, 2 m) with the (a) interpolated streamwise wind velocity flow field used in the parabolic equation (PE) model and (b) overall relative sound pressure levels (rel. SPL) computed from the PE model.

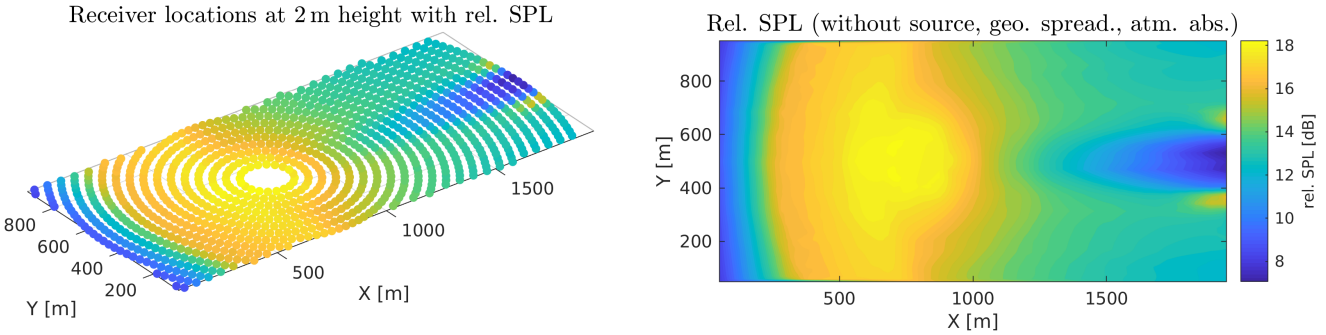

(a) (b)

Fig. 8 Mean overall relative sound pressure levels (rel. SPL) from time period 640-800 seconds shown (a) on top of the 1082 receiver locations at 2 m height and (b) as a contour plot.

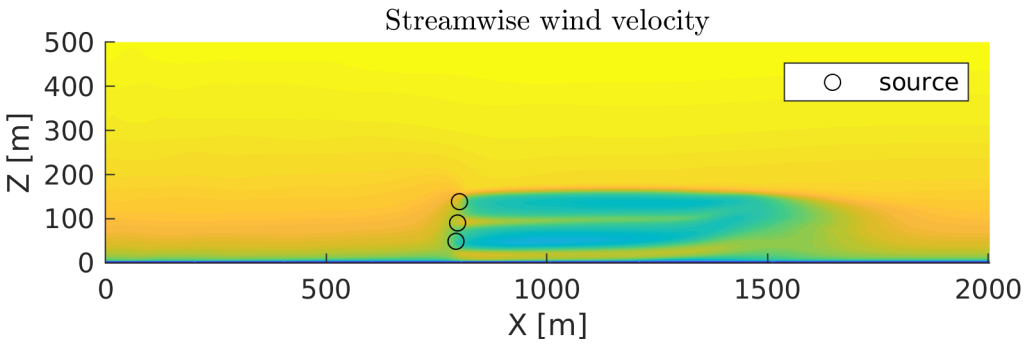

Fig. 9 Streamwise wind velocity at time = 80 seconds where the wind turbine wake does not reach the end of the domain and is not fully developed like in Figure 6(a).

the paraxial direction. The effect of the wide-angle implementation on the solution can be seen in Figure 7(b). For the NREL 5 MW wind turbine with a hub height of 90 m and a rotor radius of 63 m, the area at 2 m height with a radius of approximately [90 m + (0.8 $\times$ 63 m) - 2 m] $\times$ sin(35°) = 80 m around the turbine location in Figure 8(b) (and also Figure 10 later) should be disregarded. The contour data for all wind inflow conditions are stored in the database (or used to construct a surrogate model), which is then used in wind plant layout optimization frameworks.

Figure 10 depicts an excerpt from the noise propagation database. In Figure 10, contour plots of mean overall relative sound pressure level, i.e., mean ΔL_{sum}, from the time period 640-800 seconds are shown for a range of wind speeds (U_H) and wind shear exponents (ν): (a) U_H = 4 m/s, ν = 0.1, (b) U_H = 4 m/s, ν = 0.25, (c) U_H = 8 m/s, ν = 0.1, (d) U_H = 8 m/s, ν = 0.25, (e) U_H = 8 m/s, ν = 0.4, (f) U_H = 12 m/s, ν = 0.1, (g) U_H = 12 m/s, ν = 0.25, and (h) U_H = 12 m/s, ν = 0.4. The wind speed, U_H, is defined at hub height at the inlet, see subsection 2.3 and Equation (1). For all these cases, the turbulence intensity measured at the rotor center varies between 0.5% and 1.8%. The turbulence level in the flow can be scaled using the database parameter, K. For all cases shown in Figure 10, K = 1. Depending on the location of a particular wind turbine during a wind farm layout optimization run, the local wind conditions, e.g. U_H and ν, are extracted and used to determine the relative sound pressure level around this turbine based on the database.

Figure 11 depicts the relative sound pressure level spectra for one source/blade at time = 800 seconds upstream and downstream from the wind turbine position X, Y = (800 m, 500 m) at 2 m height for (a) U_H = 4 m/s, ν = 0.1 and (b) U_H = 12 m/s, ν = 0.1. The rel. SPL in general becomes less negative from upstream to downstream of the wind turbine. Downstream from the wind turbine, i.e., $X >$ 800 m and Y = 500 m, the peaks and troughs in the spectra suggest constructive and destructive interference of ground reflected and direct waves. Upwind of the wind turbine, i.e., $X <$ 800 m and Y = 500 m, the rel. SPL decreases smoothly for increasing frequency, f, suggesting that there is no wave interaction.

5. Conclusion

This paper described wind turbine noise propagation in flat terrain for use in wind farm layout optimization frameworks. Large-eddy simulations of a single wind turbine in flat terrain at varying wind speeds, shear and turbulence levels were performed. The wind turbine is modeled using an actuator line approach, while the wind turbine noise propagation is computed using the Technical University of Denmark's WindSTAR-Pro (Wind turbine Simulation Tool for AeRodynamic noise Propagation). The wind turbine noise propagation was computed in a quasi-three-dimensional manner by using a two-dimensional (2D) parabolic equation (PE) model at numerous 2D-planes around the wind turbine. In this study, the 2D, wide-angle, Crank-Nicholson PE model was used. The relative sound pressure level obtained from WindSTAR-Pro around the wind turbine was computed for varying wind speeds, shear and turbulence levels. Wind flow velocity and relative sound pressure levels for selected wind conditions were shown. The end goal is to create a noise propagation database that can be used as a lookup table in wind farm layout optimization frameworks to mitigate the noise impact in the development of new wind farms.

Acknowledgments

This research was funded by the Department of Wind Energy, Technical University of Denmark. Computations were performed on Jess, the high performance computing cluster at Risø Campus,

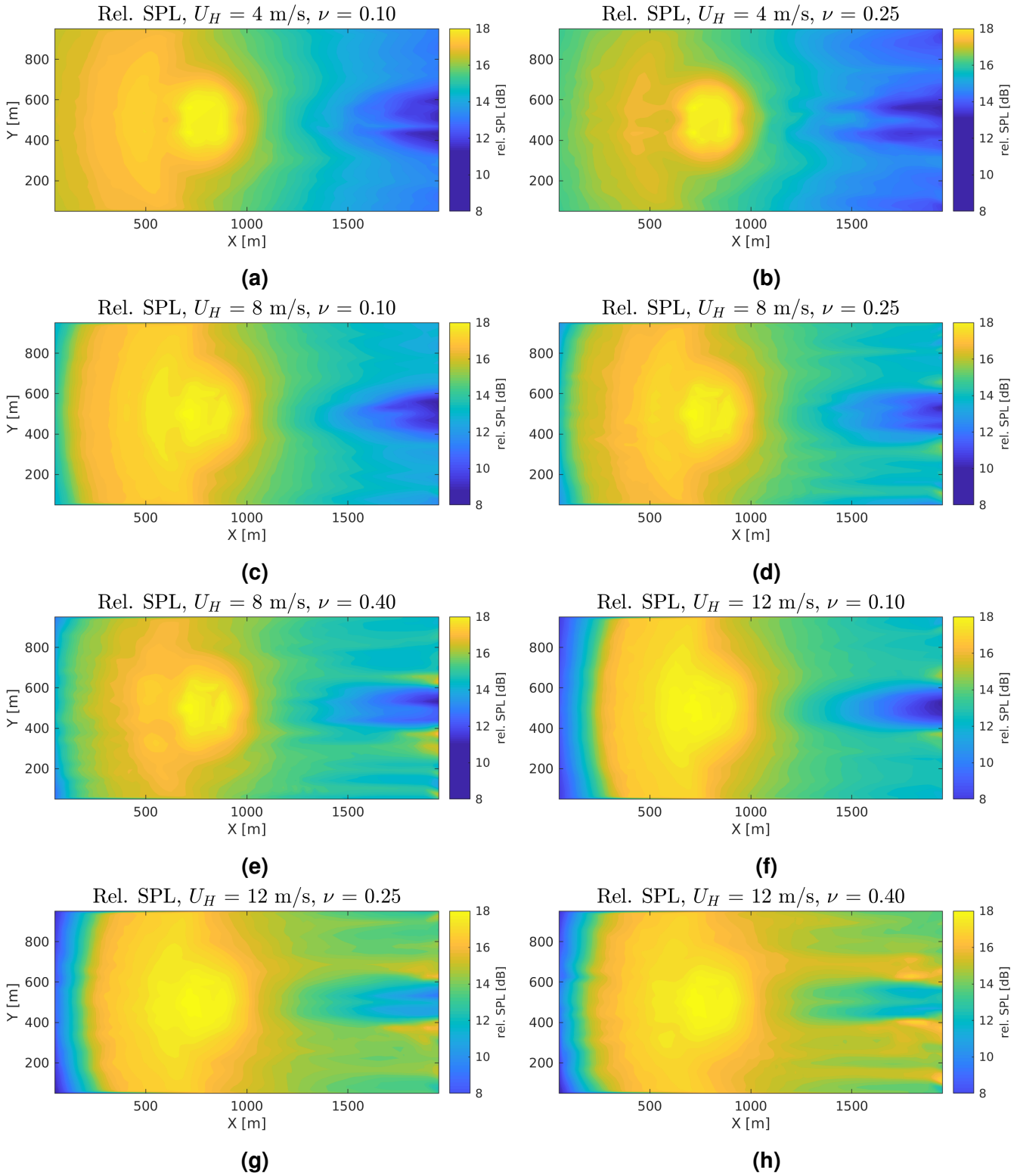

Fig. 10 Contour plots of mean overall relative sound pressure level (rel. SPL) from the time period 640-800 seconds for a range of wind speeds (U_H) and wind shear exponents (ν): (a) U_H = 4 m/s, ν = 0.1, (b) U_H = 4 m/s, ν = 0.25, (c) U_H = 8 m/s, ν = 0.1, (d) U_H = 8 m/s, ν = 0.25, (e) U_H = 8 m/s, ν = 0.4, (f) U_H = 12 m/s, ν = 0.1, (g) U_H = 12 m/s, ν = 0.25, and (h) U_H = 12 m/s, ν = 0.4.

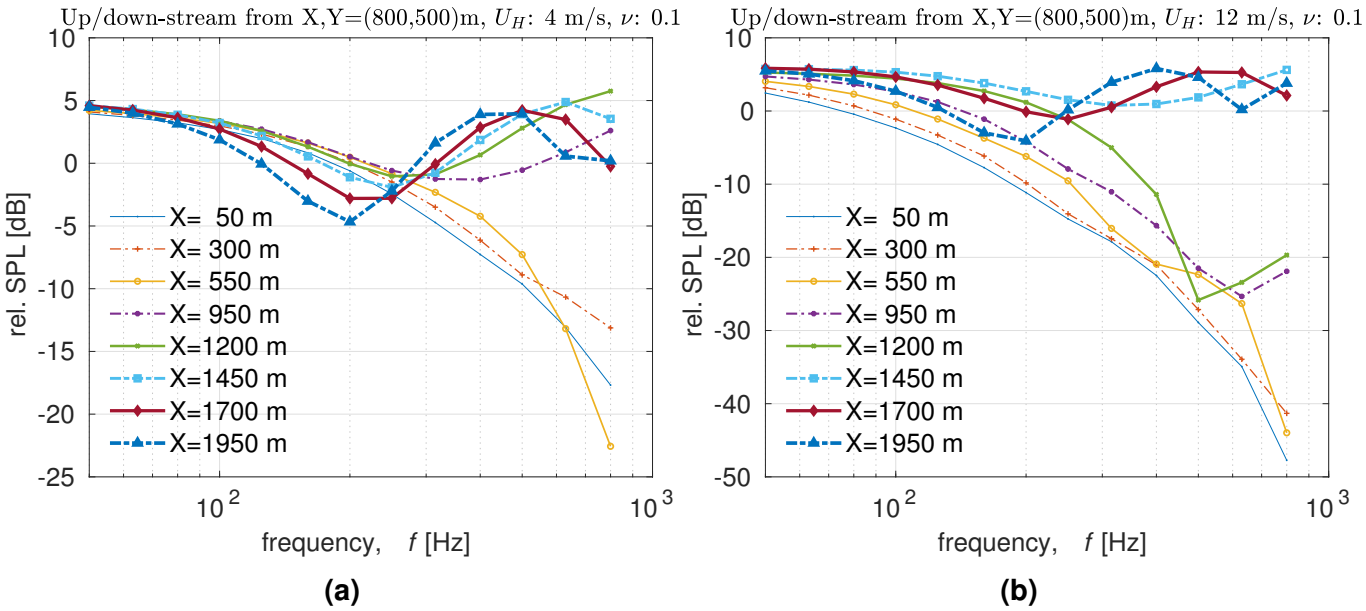

Fig. 11 Relative sound pressure level spectra for one source/blade at time = 800 seconds upstream and downstream from the wind turbine position at 2 m height for (a) U_H = 4 m/s, ν = 0.1 and (b) U_H = 12 m/s, ν = 0.1.

Technical University of Denmark.

Nomenclature

α	atmospheric absorption coefficient
ΔL	relative sound pressure level
ΔL_{sum}	overall relative sound pressure level
δx	spatial resolution for horizontal direction on 2D-plane
δy	spatial resolution for vertical direction on 2D-plane
λ	wavelength of the solving frequency
ν	wind shear exponent
c	speed of sound
c_{eff}	effective speed of sound
f	frequency
K	turbulence level scale parameter
L_p	sound pressure level
L_W	sound power level
N	number of frequencies used
r	radial distance from the source
$U(Y)$	wind speed at height Y
U_H	wind speed at hub height Y_H
v_x	wind velocity component along direction between source and receiver
X, Y, Z	location in a 3D Cartesian coordinate system
$X_{\text{length}}, Y_{\text{length}}, Z_{\text{length}}$	domain lengths in a 3D Cartesian coordinate system
$X_{\text{origin}}, Y_{\text{origin}}, Z_{\text{origin}}$	origin location in a 3D Cartesian coordinate system
$X_{\text{rotor}}, Y_{\text{rotor}}, Z_{\text{rotor}}$	rotor location in a 3D Cartesian coordinate system
2D	two-dimensional

3D	three-dimensional
AL	actuator line
BPM	Brooks, Pope, Marcolini
CFD	computational fluid dynamics
DTU	Technical University of Denmark
LES	Large-Eddy Simulation
MPI	Message Passing Interface
PE	parabolic equation
RANS	Reynolds-Averaged Navier Stokes
rel.	relative
RPM	revolutions per minute
SGS	sub-grid scale
SPL	sound pressure level
w	normalized streamwise velocity
WindSTAR-Pro	Wind turbine Simulation Tool for AeRodynamic noise Propagation

References

[1] French-Brooks, J., Smith, M., and Wiesel, J., editors (2016). *Nordic Energy Technology Perspectives 2016: Cities, flexibility and pathways to carbon-neutrality*. Nordic Energy Research, International Energy Agency, Stensberggata 25, NO-0170 Oslo, Norway.

[2] Oerlemans, S., Sijtsma, P., and López, B. M. (2007). Location and quantification of noise sources on a wind turbine. *Journal of Sound and Vibration*, 299(4):869 – 883.

[3] Pedersen, E. and Kerstin, P. W. (2004). Perception and annoyance due to wind turbine noise—a dose–response relationship. *The Journal of the Acoustical Society of America*, 116(6):3460–3470.

[4] Persson Waye, K. and Öhrström, E. (2002). Psycho-acoustic characters of relevance for annoyance of wind turbine noise. *Journal of Sound and Vibration*, 250(1):65 – 73.

[5] The Danish Ministry of the Environment (2011). Statutory order no. 1284 on noise from wind turbines.

[6] Feng, J., Shen, W. Z., and Li, Y. (2018). An optimization framework for wind farm design in complex terrain. *Applied Sciences*, 8(11).

[7] Dimitrov, N., Kelly, M. C., Vignaroli, A., and Berg, J. (2018). From wind to loads: wind turbine site-specific load estimation with surrogate models trained on high-fidelity load databases. *Wind Energy Science*, 3(2):767–790.

[8] Schröder, L., Dimitrov, N. K., Verelst, D. R., and Sørensen, J. A. (2018). Wind turbine site-specific load estimation using artificial neural networks calibrated by means of high-fidelity load simulations. *Journal of Physics: Conference Series*, 1037:062027.

[9] Brooks, T. F., Pope, D. S., and Marcolini, M. A. (1989). Airfoil self-noise and prediction. *NASA Reference publication 1218*.

[10] Amiet, R. (1975). Acoustic radiation from an airfoil in a turbulent stream. *Journal of Sound and Vibration*, 41(4):407 – 420.

[11] van der Laan, M. P., Sørensen, N. N., Réthoré, P.-E., Mann, J., Kelly, M. C., Troldborg, N., Schepers, J. G., and Machefaux, E. (2015a). An improved k- ϵ model applied to a wind turbine wake in atmospheric turbulence. *Wind Energy*, 18(5):889–907.

[12] van der Laan, M. P., Sørensen, N. N., Réthoré, P.-E., Mann, J., Kelly, M. C., and Troldborg, N. (2015b). The k-ε-f_p model applied to double wind turbine wakes using different actuator disk force methods. *Wind Energy*, 18(12):2223–2240.

[13] Sørensen, N. N. (1994). *General purpose flow solver applied to flow over hills*. PhD thesis, Technical University of Denmark.

[14] Michelsen, J. A. (1992). Basis3D - a platform for development of multiblock PDE solvers. Technical

report, Technical University of Denmark.
[15] Shen, W. Z., Michelsen, J. A., and Sørensen, J. N. (2001). Improved Rhie-Chow interpolation for unsteady flow computations. *AIAA Journal*, 39(12):2406–2409.
[16] Shen, W. Z., Michelsen, J. A., Sørensen, N. N., and Sørensen, J. N. (2003). An improved SIMPLEC method on collocated grids for steady and unsteady flow computations. *Numerical Heat Transfer, Part B: Fundamentals*, 43(3):221–239.
[17] Sørensen, J. N. and Shen, W. Z. (2002). Numerical modeling of wind turbine wakes. *Journal of Fluids Engineering*, 124(2):393–399.
[18] Sørensen, J. N., Mikkelsen, R. F., Henningson, D. S., Ivanell, S., Sarmast, S., and Andersen, S. J. (2015). Simulation of wind turbine wakes using the actuator line technique. *Philosophical transactions. Series A, Mathematical, physical, and engineering sciences*, 373(2035):20140071.
[19] Øye, S. (1996). FLEX4 simulation of wind turbine dynamics. In *Proceedings of 28th IEA Meeting of Experts Concerning State of the Art of Aeroelastic Codes for Wind Turbine Calculations*, pages 71–76, Lyngby. International Energy Agency.
[20] Jonkman, J., Butterfield, S., Musial, W., and Scott, G. (2009). Definition of a 5-MW reference wind turbine for offshore system development. Technical report.
[21] Sessarego, M., Shen, W. Z., Van der Laan, M. P., Hansen, K. S., and Zhu, W. J. (2018). CFD simulations of flows in a wind farm in complex terrain and comparisons to measurements. *Applied Sciences*, 8(5).
[22] Mann, J. (1994). The spatial structure of neutral atmospheric surface-layer turbulence. *Journal of Fluid Mechanics*, 273:141–168.
[23] Mann, J. (1998). Wind field simulation. *Probabilistic Engineering Mechanics*, 13(4):269 – 282.
[24] Hansen, M. O. L. (2008). *Aerodynamics of wind turbines*. Earthscan, London, 2nd edition.
[25] Barlas, E. (2017). *Development of an advanced noise propagation model for noise optimization in wind farm*. PhD thesis, Technical University of Denmark.
[26] Zhu, W. J., Shen, W. Z., Barlas, E., Bertagnolio, F., and Sørensen, J. N. (2018). Wind turbine noise generation and propagation modeling at DTU wind energy: A review. *Renewable and Sustainable Energy Reviews*, 88:133 – 150.
[27] Bérengier, M. C., Gauvreau, B., Blanc-Benon, P., and Juvé, D. (2003). Outdoor sound propagation: A short review on analytical and numerical approaches. *Acta Acustica united with Acustica*, 89(6):980–991.
[28] West, M., Gilbert, K., and Sack, R. (1992). A tutorial on the parabolic equation (PE) model used for long range sound propagation in the atmosphere. *Applied Acoustics*, 37(1):31 – 49.
[29] Ostashev, V. E. and Wilson, D. K. (2015). *Acoustics in Moving Inhomogeneous Media*. 2nd Edition. CRC Press.
[30] Barlas, E., Zhu, W. J., Shen, W. Z., Kelly, M., and Andersen, S. J. (2017a). Effects of wind turbine wake on atmospheric sound propagation. *Applied Acoustics*, 122:51 – 61.
[31] Barlas, E., Zhu, W., Shen, W., Dag, K., and Moriarty, P. (2017b). Consistent modelling of wind turbine noise propagation from source to receiver. *Acoustical Society of America. Journal*, 142(5).
[32] Barlas, E., Wu, K. L., Zhu, W. J., Porté-Agel, F., and Shen, W. Z. (2018). Variability of wind turbine noise over a diurnal cycle. *Renewable Energy*, 126:791 – 800.
[33] Attenborough, K. (1985). Acoustical impedance models for outdoor ground surfaces. *Journal of Sound and Vibration*, 99(4):521 – 544.